American Mineralogist, Volume 94, pages 710–719, 2009

Synchrotron-based speciation of chromium in an Oxisol from New Caledonia: Importance of secondary Fe-oxyhydroxides

Dik Fandeur,[1,*] Farid Juillot,[1] Guillaume Morin,[1] Luca Olivi,[2] Andrea Cognigni,[2] Jean-Paul Ambrosi,[3] François Guyot,[1] and Emmanuel Fritsch[1]

[1]Institut de Minéralogie et de Physique des Milieux Condensés (IMPMC), Université Pierre et Marie Curie, Université Paris Diderot, IPGP, UMR CNRS 7590, Campus Boucicaut, 75015, Paris, France
[2]Sincrotrone Trieste (ELETTRA), Area Science Park, Strada Statale, 34012 Basovizza, Trieste, Italy
[3]Institut de Recherche pour le Développement (IRD), UMR 161, BP A5, 98848 Nouméa, New Caledonia

Abstract

In New Caledonia, the weathering of ultamafic rocks under a tropical climate has led to the residual accumulation of trace elements in lateritic soils widely dominated by Fe-oxyhydroxides. The speciation of trace elements, such as Cr, Ni, and Co, in these Oxisols remains a major subject of interest regarding mining and environmental issues. We have assessed the speciation of chromium in the upper part of an Oxisol, by combining bulk and spatially resolved chemical analyses (EPMA and SEM-EDS) with synchrotron-based spectroscopic data (EXAFS and XANES). EPMA indicates that the main hosts for chromium in the bedrock sample are the silicates forsterite, enstatite, and lizardite. Hosting of chromium in these easily weatherable mineral species could lead to a significant loss of this element upon weathering. However, total analyses of major elements indicate only a slight depletion of Cr, together with an immobility of Fe and Al and drastic losses of Si and Mg, after the weathering of the bedrock. Such a low mobility of chromium is likely related to its significant incorporation in goethite and hematite formed after the weathering of Fe^{2+}-bearing primary silicates. This efficiency of secondary Fe-oxyhydroxides at immobilizing chromium is demonstrated by quantitative analysis of EXAFS data that indicates that these mineral species host between 67 and 75 wt% of total Cr (compared to the 18 to 22 wt% of total Cr hosted by chromite). In addition, SEM observation and SEM-EDS analyses performed on the Oxisol samples also show some evidence for chemical weathering of chromite. Chromite could then represent a past and/or present source of chromium upon extended tropical weathering of the studied Oxisol, rather than a stable host. These results emphasize the importance of secondary Fe-oxyhydroxides, compared to Cr-spinels, on chromium hosting in Oxisols developed upon tropical weathering of ultramafic rocks. Although the trapping mechanism of chromium mainly corresponds to incorporation within the structural network of goethite and hematite, sorption reactions at the surface of these mineral species could also be involved in such a process. In addition, considering their potential oxidative reactivity that can generate Cr^{6+} or enhance the chemical weathering of chromite, the occurrence of Mn oxides could significantly modify the behavior of chromium upon weathering. These considerations indicate that further studies are needed to assess the actual potential of chromium release from Oxisols developed upon weathering of ultramafic rocks under a tropical climate.

Keywords: Chromium, speciation, Oxisol, New Caledonia

Introduction

New Caledonia is well known for the endemic character of its fauna and flora (Myers et al. 2000; Proctor 2003). One third of the island is covered with ultramafic rocks (Coleman 1980) and intense weathering of these rocks under a tropical climate has led to the formation of deep lateritic soils, also known as Oxisols. Compared to their parent materials, these Oxisols are strongly depleted in soluble elements like Ca, Mg, and Si, and enriched in weakly mobile elements, mainly Fe and, to a lesser extent, Al (Perrier et al. 2006; Becquer et al. 2006). Among the weakly mobile elements, potentially toxic trace elements like Ni and Cr can reach concentration up to several wt% in Oxisols (Becquer et al. 2006), whereas their average concentration in the Earth's crust is only 100 mg/kg (Nriagu 1988). Although Ni is known to severely restrict plant growth in Ni-enriched soils (Weng et al. 2004; Rooney et al. 2006), the major concern with these large concentrations of trace elements in Oxisols comes from Cr, which is considered as one of the 14 most toxic metals, especially concerning its carcinogenic character (Fendorf 1995). High levels of Cr in Oxisols can then be very hazardous for the environment depending on its toxicity, mobility, and bioavailability. For Cr, these properties are largely controlled by its redox state. Reduced Cr (Cr^{3+}) is non-hazardous and has a low solubility [$Ks = 10^{-30}$ for $Cr(OH)_3$ according to Garrels and Christ 1965]. It can substitute for Fe and/or Mn in oxides or sorb onto their surface (Fendorf 1995; Becquer et al. 2003), which makes this

* E-mail: dik.fandeur@impmc.jussieu.fr

form less harmful for the environment. In contrast, oxidized Cr (Cr^{6+}) is more toxic and has a larger solubility, which makes this form more prejudicial for the environment (Fendorf 1995). This contrasted behavior between Cr^{3+} and Cr^{6+} indicates that accurate estimation of the environmental risk associated with the occurrence of large amounts of Cr in Oxisols is strongly dependent on our capacity to identify the actual crystal chemistry of this element in these surface environments.

Several studies have already focused on the crystal chemistry of Cr in soils developed upon mafic and ultramafic rocks under various weathering conditions (Becquer et al. 2003, 2006; Oze et al. 2004a, 2007; Doelsch et al. 2006; Garnier et al. 2006; Soubrand-Colin et al. 2007). In the case of slight weathering under a temperate or Mediterranean climate, moderate leaching of very soluble Mg and less soluble Si lead to a significant fraction of these elements remaining in the soil, to subsequently react together to precipitate as secondary Cr-bearing Mg-clays, like smectite and vermiculite, or chromite/silicate mixtures (Oze et al. 2004a; Soubrand-Colin et al. 2007). However, considering the large amounts of chromite ($FeCr_2O_4$) and Cr-magnetite ($FeFe_{2-x}Cr_xO_4$) inherited from the parent materials and their high Cr content, secondary Cr-bearing silicates do not represent the main host for Cr in these soils developed upon slight weathering of mafic and ultramafic rocks (Oze et al. 2004a; Soubrand-Colin et al. 2007). According to Oze et al. (2004a), Cr-spinels are so predominant as Cr hosts that they control the distribution of Cr in the serpentinite soils from Jasper Ridge (California, U.S.A.). The situation is quite different in the case of deep weathering under tropical conditions, when soluble Mg and Si have been almost totally leached and only non-soluble elements like Fe, Al, Mn, and Cr remain in the Oxisols. In such situations, these elements subsequently precipitate as Cr/Al-bearing Fe-oxyhydroxides, mainly goethite (α-FeOOH) and hematite (α-Fe_2O_3), which coexist with Cr-bearing spinels inherited from the bedrock (Becquer et al. 2003, 2006; Doelsch et al. 2006; Garnier et al. 2006). Considering the large amounts of Cr-bearing Fe-oxyhydroxides and their significant Cr concentration (up to 2.6 mol% Cr_2O_3, according to Becquer et al. 2003), these secondary minerals might even represent major host for Cr compared to Cr-spinels in these Oxisols. Although the relative solubility of Fe-oxyhydroxides and spinels in oxidized soil conditions is quite similar (Cornell and Schwertmann 2003), the knowledge of the actual partitioning of Cr between these two kinds of minerals can bring useful information on its behavior upon weathering and pedogenesis. However, up to now, the only study reporting an in situ quantitative analysis of the relative proportions of Cr hosted in secondary Cr-bearing Fe-oxyhydroxides and in primary Cr-spinels indicated a major contribution of chromite in the different granulometric fractions of an Andosol developed under the tropical climate of the volcanic island of Réunion (Doelsch et al. 2006). All these considerations indicate that further in situ studies are needed to better characterize Cr speciation in soils developed upon tropical weathering of ultramafic rocks and to better estimate the relative importance of relict primary and secondary Cr-bearing minerals on the total budget of Cr in these specific environments.

This study aims to establish an in situ quantitative crystal-chemistry of Cr along the upper part of a New Caledonian Oxisol to evaluate the relative importance of the various Cr-bearing minerals on the sequestering of Cr upon tropical weathering of ultramafic rocks. In a first step, spatially resolved chemical analyses (EPMA and SEM-EDS) were used to identify the various Cr-bearing minerals in the studied Oxisol. In a second step, linear combination of EXAFS spectra of selected reference compounds was performed to quantify the partitioning of Cr between these various Cr-bearing minerals. In addition, considering the possible redox reactivity of Cr with various soil components (Manceau and Charlet 1992; Fendorf et al. 1993; Fendorf and Li 1996; Peterson et al. 1997; Kendelewicz et al. 2000; Loyaux-Lawniczak et al. 2000; Williams and Scherrer 2001; Szulczewski et al. 2001; Weaver and Hochella 2003; He et al. 2005; Feng et al. 2006; Murray and Tebo 2007; Oze et al. 2007), the evolution of the oxidation state of Cr along the studied Oxisol was followed by XANES spectroscopy to emphasize a possible control of the weathering reactions on this key parameter for Cr geochemical behavior. All these results yield useful information to better understand the geochemical behavior of chromium upon tropical weathering of ultramafic rocks and to estimate the risk associated to the occurrence of large amounts of Cr in Oxisols.

Materials and experimental methods

Site location and sample selection

The first 2 m of an Oxisol developed on ultramafic rocks was selected for this study (20°59' S, 164°49' W). This Oxisol belongs to the downslope part of a soil catena, previously investigated by Perrier et al. (2006), which caps at 900 m the Koniambo massif (West side of the Grande Terre island in the Northern Province), on the eastern side of the Pandanus watershed (Perrier et al. 2006). The massif is mainly composed of harzburgite crossed by serpentine veins, with some outcrops of dunite and gabbro intrusions (Perrier et al. 2006). Similar types of soils, referred as Oxisols (USDA Soil Taxonomy) or Ferralsols (World Reference Base for Soil Resources), are observed along the whole toposequence. They are predominantly made of small ironstone nodules (<4 mm) and are characteristic of freely drained soils. The nodules are closely associated with a small proportion of fine material, which is sparse in the upper part of the soils. The investigated Oxisol is composed of loose materials and is homogeneous in texture (<10% of silt and clay) and color that ranges from yellowish red (5 YR 4/6 on dry samples) to strong brown (7.5 YR 5/8 on dry samples). Three Oxisol samples at 10, 80, and 160 cm depth and one sample of unweathered peridotite, which constitutes the bedrock of the weathering sequence of the Koniambo massif, were sampled and subsequently analyzed for their chemical and mineralogical composition (Table 1). The pH of these soil samples was measured in suspensions with a solid/liquid ratio of 1 g/10 mL, after 10 min shaking and 30 min settling. Measured pH values are 5.3 (10 cm), 4.7 (80 cm), 5.0 (160 cm), and 8.6 (bedrock).

Table 1. ICP-OES analyses (wt% oxides) of studied samples after alkali fusion with lithium tetraborate

Sample	SiO_2	MgO	Fe_2O_3	Cr_2O_3	Al_2O_3	MnO	NiO	TiO_2	Total	pH	T.O.C.*
Oxisol											
10 cm	2.1	0.4	72.6	2.2	5.6	0.3	0.5	0.1	98.5	5.3	19.7
80 cm	2.0	0.8	70.0	2.0	7.4	0.3	0.7	0.1	97.8	4.7	4.0
160 cm	2.2	0.7	69.6	1.4	6.5	0.4	0.8	0.1	96.3	5.0	3.8
Bedrock	40.0	44.0	8.5	0.3	0.7	0.1	0.5	0.0	99.3	9.6	n.d.†

* Total organic carbon.
† Not determined.

Chemical and mineralogical characterization by ICP-OES, SEM-EDS, EPMA, and XRD

Concentrations of major (SiO_2, MgO, Fe_2O_3, Al_2O_3, TiO_2, K_2O, CaO, Na_2O, MnO, and P_2O_5) and trace (Ni, Co, Zn, Cu, Cr, and V) elements in the samples were determined by ICP-OES, with a Perkin Elmer optima 3300 DV, after alkali fusion with lithium tetraborate at the Centre Européen de Recherche et d'Enseignement des Géosciences de l'Environnement (CEREGE, Aix en Provence, France). Spatially resolved observations and chemical analyses were performed by scanning electron microscopy (SEM) and electron microprobe analyses (EPMA). Because of their low cohesion, samples to be analyzed were first embedded in a Mecaprex resin before being hand-polished and coated with a thin carbon film. SEM observations and analyses were performed with a LEO Stereoscan 440 equiped with an energy dispersive spectrometer (EDS) for chemical analyses and operating at 20 kV and 150 pA at the Laboratoire Interfaces et Systèmes Electrochimiques (LISE, Université Pierre et Marie Curie, Paris France). EPMA were performed with a CAMECA SX50 equipped with four wavelength dispersive spectrometers (WDS) and operating at 15 kV and 30 nA at the Centre d'Analyze des Minéraux de PARIS (CAMPARIS, Université Pierre et Marie Curie, Paris, France).

Mineralogical compositions of the samples were assessed by powder X-ray diffraction (XRD) with a Philips PW 1730 using Co$K\alpha$ radiation and operating at 40 kV and 30 mA at the Institut de Minéralogie et de Physique des Milieux Condensés (IMPMC, Paris, France). XRD patterns were collected for 2θ angles ranging from 3 to 90° with a 0.03° step size and a counting time of 15 s per step. Before these mineralogical analyses, samples were manually ground to powders (±30 μm) in an agate mortar and prepared according to the technique of the "back pack-mounted slide" (Bish and Reynolds 1989).

Crystal-chemistry of Cr by synchrotron-based X-ray absorption spectroscopy

Data collection and processing. The Cr *K*-edge XAS experiments were performed on the bending magnet XAFS beamline at the ELETTRA Synchrotron Light Source (Trieste, Italy). Samples were prepared as self-supported films (Oxisol samples) or pellets (model compounds) of finely hand-ground and homogenized powders. All data were collected at room temperature and in transmission mode using ion chambers filled with various mixtures of He-N_2-Ar. The energy of the X-ray beam was tuned with a Si(111) double-crystal monochromator, which yielded an energy resolution around 0.8 eV at the Cr *K*-edge (5989 eV for metallic Cr). The size of the X-ray beam on each sample was 3 × 8 mm. Data were collected in the range 5950–6140 and 5900–6500 eV for XANES and EXAFS, respectively. EXAFS data could not be collected at higher energy due to the occurrence of the Mn *K*-edge (6539 eV for metallic Mn) in the EXAFS spectra of all Oxisol samples. For all experiments, the threshold energy was calibrated by setting the first maximum of the first derivative of the XANES spectrum of a Cr metal foil at 5989 eV. Depending on the Cr concentration in the sample and on the energy range scanned, 2–12 scans were necessary to obtain a good signal-to-noise ratio. All the scans registered for a given sample were averaged using the ATHENA code (Ravel and Newville 2005). Each average scan was then processed with the XAFS code (Winterer 1997) to extract the χ(k) function by subtracting a linear function and a spline function to the experimental data before and after the edge, respectively. Each edge-jump was then normalized to unity and the abscissa of the resulting spectrum was converted from energy (eV) to photoelectron wave vector ($Å^{-1}$) by setting the energy threshold at the first inflection point of each spectrum. EXAFS spectra obtained with this procedure were k^3-weighted to attenuate the dampening of oscillations due to the k-dependence of the backscattering of the photoelectron by neighboring atoms.

Quantitative speciation of Cr by least-squares fitting analysis of EXAFS data. Unsmoothed k^3-weighted experimental EXAFS spectra of the studied Oxisol samples were analyzed by a linear combination least-squares fitting (LC-LSF) procedure (Scheinost et al. 2002; Isaure et al. 2002; Voegelin et al. 2005; Sarret et al. 2004) with the SIXPACK code (Webb 2004). This procedure is based on the mathematical reconstruction of an experimental EXAFS spectrum with a linear combination of EXAFS spectra of natural or synthetic model compounds where the molecular environment of the studied element is known. The principal component analysis (PCA), which is being more and more used instead of the LSF procedure to select the model compounds possibly contributing to the analyzed experimental EXAFS spectra, was not used here due to the strong similarity between all the experimental EXAFS spectra of the studied Oxisol samples. The LC-LSF procedure results in a quantitative analysis of the different contributions of the model compounds that likely constitute the analyzed experimental EXAFS spectra. During the LC-LSF procedure, the sum of all the contributions of the model compounds in each studied Oxisol sample was set free and the E_0 value of each experimental EXAFS spectrum was not allowed to change. The accuracy of the LC-LSF procedure is assumed to range between ±25 and ±5% of the stated values of each individual contribution, depending on the quality of the experimental data and on the occurrence of distinctive features (Ostergren et al. 1999; Manceau et al. 2000; Isaure et al. 2002; Sarret et al. 2004). In our case, the accuracy of the LC-LSF procedure used was assumed to be ±10% and contributions below this value are considered as doubtful.

Redox state of Cr by XANES spectroscopy. XANES spectroscopy can be used to identify the redox of Cr because the difference in the coordination chemistry of octahedral Cr^{3+} and tetrahedral Cr^{6+} yields a different X-ray absorption behavior. Indeed, the non-centrosymmetric tetrahedral environment of Cr^{6+} yields $1s \rightarrow 3d/2p$ electric dipole transitions thanks to $3d/2p$ orbital mixing between $3d$ levels of Cr and $2p$ levels of O ligands (Peterson et al. 1997; Huggins et al. 1998). The XANES spectrum of Cr^{6+} is then characterized by the occurrence of a strong absorption peak in the pre-edge region (around 5993 eV). In the case of the centrosymmetric octahedral environment of Cr^{3+}, the absence of orbital mixing hinders these electric dipole transitions, but $1s \rightarrow 3d$ electric quadrupole transitions are possible due to the occurrence of empty $3d$ levels arising from the d^3 configuration of Cr^{3+}. Because of the splitting of the $3d$ levels in t_{2g} and e_g and considering both spin up and spin down final states, three sets of electronic transitions are possible (Gaudry et al. 2007; Juhin et al. 2008). However, because of the similar energy between two of these transitions, the XANES spectrum of Cr^{3+} is characterized by the occurrence of only two weak peaks (at 5990 and 5993 eV) in the pre-edge region (Gaudry et al. 2007; Juhin et al. 2008). The intensity of the peak at 5990 eV is usually higher than that of the peak at 5993 eV, but structural distortion of the octahedral site of Cr^{3+} can yield a loss of symmetry and then favor the $3d/2p$ orbital mixing between $3d$ levels of Cr and $2p$ levels of O ligands, as in the case of non-centrosymmetric tetrahedral Cr^{6+}. Distortion of the octahedral environment of Cr^{3+} can then yield $1s \rightarrow 3d/2p$ electric dipole transitions, which result in an increase of the intensity of the pre-edge peak at 5993 eV. In addition to a simple identification of the redox state of Cr, XANES spectroscopy can also be used to quantify the Cr^{6+}/Cr^{3+} ratio in unknown samples, after calibration of the method on synthetic samples where this ratio is known (Huggins et al. 1998).

Model compounds for XAS analyses. Several synthetic or natural model compounds were used to analyze XAS data. Among natural model compounds were a chromite and a Cr-bearing serpentine. The chromite sample resulted from a densimetric separation of sediments collected in the Pandanus River. The Cr-bearing serpentine sample occurred as a coating of a harzburgite rock sample at the bottom of the weathering sequence of the Koniambo massif and was likely related to a past large vein that has been exposed to the air after Ni ore mining works. Among synthetic samples were Cr-bearing goethite and hematite prepared by co-precipitating Cr^{3+} and Fe^{3+} following the method of Cornell and Schwertmann (2003). For Cr-bearing goethite, 23.75 mL of a 1 *M* $Fe(NO_3)_3$-$9H_2O$ solution were mixed with 1.25 mL of a 1 *M* $Cr(NO_3)_3$-$9H_2O$ solution and 45 mL of a 5 *M* KOH solution into a 500 mL polyethylene flask under rapid stirring. The mixed solution was immediately completed to 500 mL with double-distilled water and aged at 70 °C for 60 h. For hematite, 38.87 g of $Fe(NO_3)_3$-$9H_2O$ and 1.285 g of $Cr(NO_3)_3$-$9H_2O$ were dissolved in 500 mL of double-distilled water preheated to 90 °C. The solution was neutralized with 1 *M* KOH, also preheated to 90 °C. The suspension was then aged at 90 °C during 48 h. In both cases, after aging, the supernatants and the solids of the suspensions were separated by ultra-centrifugation at 15 000 rpm for 30 min. The solids collected were washed three times with double-distilled water and dried at 40 °C for 8 h. After both syntheses, possible unwanted ferrihydrite was removed by reacting the solids with a 0.2 *M* $(NH_4)_2C_2O_4 \cdot H_2O/H_2C_2O_4$ solution (Quantinet al. 2002). This reaction was performed at pH 3 with a solid/liquid ratio of 1/10 for 4 h, under constant stirring in the dark. Finally, both synthetic Cr-bearing Fe-oxyhydroxides were reacted with a 0.1 *M* $CaCl_2$ solution during 2 h to desorb possibly sorbed Cr. After both treatments, the reacted solids were ultra-centrifuged at 15 000 rpm for 30 min, washed 3 times with double-distilled water and dried at 40 °C for 8 h.

Results and discussion

Bulk concentrations of major elements and chromium in the studied samples

Concentrations of Mg, Si, Cr, Al, and Fe along the investigated Oxisol and in the bedrock sample are shown in Table 1. The bedrock sample exhibits high Mg and Si concentrations

(about 44 wt% MgO and 40 wt% SiO_2), low Fe concentrations (about 8.5 wt% Fe_2O_3), and very low Al concentrations (<1 wt% Al_2O_3). In contrast, all the Oxisol samples show very low Mg and Si concentrations (<1 wt% MgO and ~2.2 wt% SiO_2), moderate Al concentration (about 7 wt% Al_2O_3), and very high Fe concentrations (~70 wt% Fe_2O_3). Chromium concentrations also show a chemical contrast between the bedrock and the Oxisol samples with an increase from about 0.3 wt% Cr_2O_3 in the bedrock up to 2.2 wt% Cr_2O_3 in the Oxisol.

Identification and chemical composition of the various Cr-bearing phases

In the bedrock sample. The XRD spectrum of the bedrock sample (Fig. 1) reveals the occurrence of three (Mg,Fe)-silicates: olivine, pyroxene, and serpentine. According to the relative intensities of the XRD peaks, olivine is the main primary mineral of the bedrock, followed by pyroxene and serpentine (Fig. 1). Electron microprobe analyses (EPMA) on polished thin sections indicate that olivine is forsterite [$(Mg_{1.79}Fe_{0.17}Ni_{0.01})Si_{1.01}O_4$], pyroxene is enstatite [$(Mg_{0.87}Fe_{0.08}Al_{0.04}Ca_{0.02}Cr_{0.01})SiO_3$] and serpentine is lizardite [$(Mg_{2.2}Fe_{0.3}Ni_{0.09}Al_{0.07}Cr_{0.02}Ca_{0.02})Si_{2.05}O_5(OH)_4$]. This mineralogical composition is in full agreement with the known peridotitic nature of the bedrock (Perrier et al. 2006).

In addition to these (Mg,Fe)-silicates, optical observations and EPMA analyses allow identification of spinels that could not be detected by XRD in the bedrock sample, likely because of their small concentration. Under the scanning electron microscope (SEM), these spinels appear as euhedral grains with a size around 100 μm. They are easily recognizable from the surrounding (Mg,Fe)-silicates because they appear much brighter in the backscattered-electron mode, which emphasizes the predominance of cations heavier than silicon and magnesium in their crystal lattice (Fig. 2). EPMA analyses indicate that these spinels are Mg/Al-rich chromites [$(Fe_{0.39}Mg_{0.60}Mn_{0.01})(Cr_{1.01}Al_{0.98})O_4$].

In the Oxisol samples. All the Oxisol samples are mainly made of millimeter-sized sub-spherical ironstone concretions (Fig. 3). These samples display a very similar mineralogical composition, which strongly differs from that reported for the bedrock sample. According to XRD data, the upper part of the Oxisol profile is largely dominated by goethite (α-FeOOH) (Fig. 1). It also contains minor amounts of hematite (α-Fe_2O_3) and spinels. EPMA indicate that the chemical composition of these secondary Fe-oxyhydroxides is slightly variable in the different Oxisol samples with mean structural formulae estimated as $(Fe_{0.85}Al_{0.09}Cr_{0.03})OOH$ for goethite and as $(Fe_{1.78}Al_{0.1}Cr_{0.08})O_3$ for hematite.

Such an occurrence of secondary Al-poor Fe-oxyhydroxides in the Oxisol samples is characteristic of the weathering of ultramafic rocks (Schwertmann and Latham 1986; Quantin et al. 2002; Becquer et al. 2001). It indicates that Mg and Si from the primary silicate minerals in the bedrock (forsterite, enstatite, and lizrardite) were strongly leached upon weathering, whereas Fe and Al remain in the weathering products (Oxisol samples) where they precipitated as secondary Al-poor Fe-oxyhydroxides. This different leaching behavior for Mg and Si, on the one hand, and

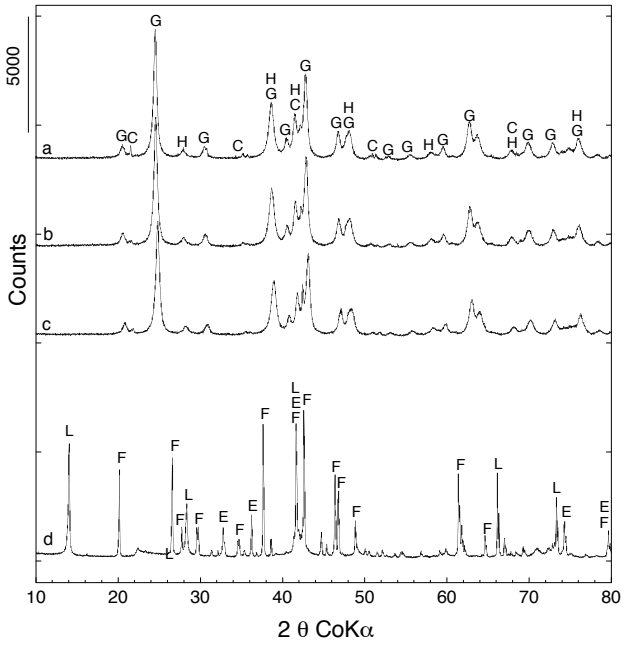

Figure 1. XRD powder patterns of the studied samples [(**a**) 10 cm, (**b**) 80 cm, (**c**) 160 cm, and (**d**) bedrock]. L = Lizardite, F = Forsterite, E = Enstatite, G = Goethite, H = Hematite, and C = Chromite.

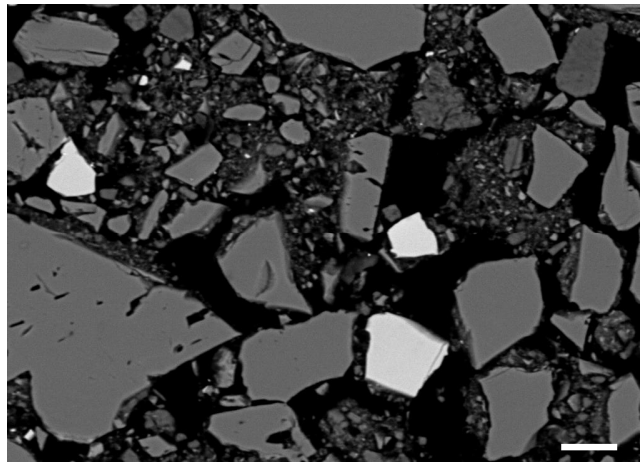

Figure 2. SEM-BSE image of bulk material from the bedrock sample. The chromite grains appear brighter than silicates because of their larger contents in Fe and Cr. Scale bar is 10 μm.

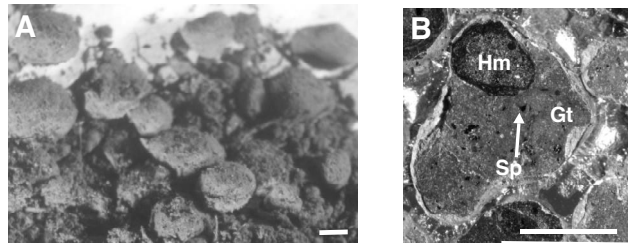

Figure 3. Optical images of bulk material (**a**) and a polished section of millimetric nodules embedded in an epoxy resin (**b**) of the Oxisol samples. Part **a** shows the nodular nature of the Oxisol samples, and part **b** emphasizes their heterogeneities with a brownish goethitic matrix (Gt), dark hematitic areas (Hm), and small opaque brilliant grains of spinels (Sp). Scale bar is 1 mm for both photomicrographs.

Fe and Al, on the other hand, is in agreement with the chemical variations observed between the bedrock sample and the Oxisol samples (Table 1). The occurrence of cations (e.g., Al and Cr) substituted for Fe within the lattice of Fe-oxyhydroxides is very common in tropical soils (Cornell and Schwertmann 2003). The average substitution rates found in this study are similar to those already reported by Quantin et al. (2002) and Becquer et al. (2001) in Oxisols developed on similar geologic formations from the Southern Province of New Caledonia. The Al substitution rates appear weak for hematite and goethite (3.0 and 5.0 wt% Al_2O_3, respectively) compared to the maximum ones commonly reported in the literature (15 and 33 mol% for hematite and goethite, respectively). However, these rates are in agreement with the development of the studied Oxisol on an Al-poor bedrock (peridotite). The Cr substitution rates are equivalent in hematite and goethite (3.2 and 2.6 wt% Cr_2O_3, respectively). These rates appear much higher than those measured in enstatite and lizardite in the bedrock. Such a relative enrichment of Cr in Cr-hosting minerals from the bedrock sample to the Oxisol samples is likely related to the efficiency of the trapping process within secondary Fe-oxyhydroxides (goethite and hematite). Such a process is then directly responsible of the low mobility of Cr observed when comparing the chemical composition of the bedrock sample and the Oxisol samples (Table 1).

XRD powder patterns of the Oxisol samples also indicate the occurrence of spinel phases, whereas XRD could not detect these phases in the bedrock sample (Fig. 1). These different amounts of spinel phases between the bedrock sample and the Oxisol samples is likely related to a relative enrichment of these minerals in the Oxisol compared to the bedrock. This relative enrichment is due to the stronger resistance of the spinel phases to chemical weathering compared to the primary (Mg,Fe)-silicates of the bedrock sample. EPMA data indicate that the spinel phases in the Oxisol samples correspond to chromite. However, in the Oxisol samples, a careful analysis of these spatially resolved chemical analyses emphasizes the occurrence of two distinct populations of chromite. The first one consists of Mg/Al-rich chromites [$(Mg_{0.52}Fe_{0.4}Mn_{0.01})(Cr_{1.16}Al_{0.89})O_4$ as the mean structural formula], which appear very similar to the Mg/Al-rich chromites identified in the bedrock. The second population of chromite consists of Mg/Al-poor chromites [$(Mg_{0,35}Fe_{0,51}Mn_{0,01})(Cr_{1,9}Al_{0,2})O_4$ as the mean structural formula]. Although known for its weak susceptibility to chemical weathering, this occurrence of two populations of chromite differing in their Al and Mg concentrations in the Oxisol raises the question of the long-term stability of this mineral species when subjected to tropical weathering.

Evidences for chemical weathering of chromite in the Oxisol samples

The contrasted concentrations of Al and Mg in the two populations of chromite in the Oxisol samples could be inherited from the peridotites as fractional crystallization of the silicate melt in the magma chamber can produce minerals with a significant compositional range. However, only the Mg/Al-rich chromites could be identified in the bedrock sample, which suggests that the Mg/Al-poor chromites recognized in the Oxisol samples likely result from incongruent dissolution of the Mg/Al-rich ones. Such a process would lead to a preferential leaching of more soluble Al and Mg and a relative enrichment of insoluble Fe and Cr in residual mineral phases, as already proposed by Oze et al. (2004a), who also observed both populations of chromite in weathering products of serpentinites from California. This preferential leaching of Al and Mg from the Mg/Al-rich chromites of the bedrock and residual accumulation of Mg/Al-poor chromites in the Oxisol is also compatible with a study of Merkle et al. (2004), who observed an important release of Al and Mg, while Fe and Cr remained in a residual phase during lithium tetraborate fluxing of the Al- and Mg-rich AG-2 chromite from the Bushveld Complex. EPMA derived chemical compositions of the two populations of chromite in the Oxisol then indicates that these minerals are subject to chemical weathering. Such chemical weathering of chromite in the Oxisol samples is also supported by SEM observations, which reveal some chromite grains with distinctive dissolution features filled with Fe-oxyhydroxides (Fig. 4).

Considering the probable release of Cr during such a chemical process, the weathering of chromite could play a significant role on the actual speciation of Cr in the studied Oxisol samples. Consequently, accurate observations and analyses were performed in the surroundings of weathered chromite grains to detect the micrometer-scale changes in the speciation of chromium induced by such weathering.

Micrometer-scale behavior of chromium upon chemical weathering of chromite

SEM observations in BSE mode of some highly porous grains of chromite surrounded by several rims of weathered materials are displayed on Figure 5. SEM-EDS analyses performed in the central part of one of these grains show a chemical composition (23.7 wt% FeO, 65.7 wt% Cr_2O_3, 5.3 wt% Al_2O_3, and 4.3 wt% MgO; Table 2) similar to that obtained by EPMA on other Mg/Al-poor chromite grains. From the inner to the outer rims of these grains (Fig. 5), the EDS analyses also reveal an increase of the Fe concentration from about 38 to 91 wt% FeO, and a decrease of Cr concentration from about 50 to 3 wt% Cr_2O_3 (Table 2). These observations suggest that the central chromite grain is the relict part of a much larger chromite grain, which underwent significant dissolution. Such dissolution of chromite has already been shown by Traoré et al. (2008) on hand-picked chromite grains collected in another soil from New Caledonia. However, our observations and analyses yield further insights into the actual mechanism (congruent vs. incongruent dissolution) involved. Since the successive rims observed on Figure 5 correspond to more and more weathered chromite when going outward from the central relict grain, the decrease in Cr and the concomitant increase in Fe from the central relict grain to the outer rim (Table 2) strongly suggests that the dissolution process corresponds to an incongruent dissolution of chromite marked by a preferential release of Cr compared to Fe. To our knowledge, this is the first time that incongruent dissolution of chromite grains marked by a preferential release of Cr compared to Fe has been shown in situ in soils. Oze et al. (2007) already reported such a contrasted behavior for Cr and Fe during the dissolution of chromite, but their results concerned experimental dissolution of chromite in the presence of birnessite, a common Mn oxide. In this study, the preferential release of Cr compared to Fe was considered as resulting from the oxidative capacity of Mn oxides, which lead

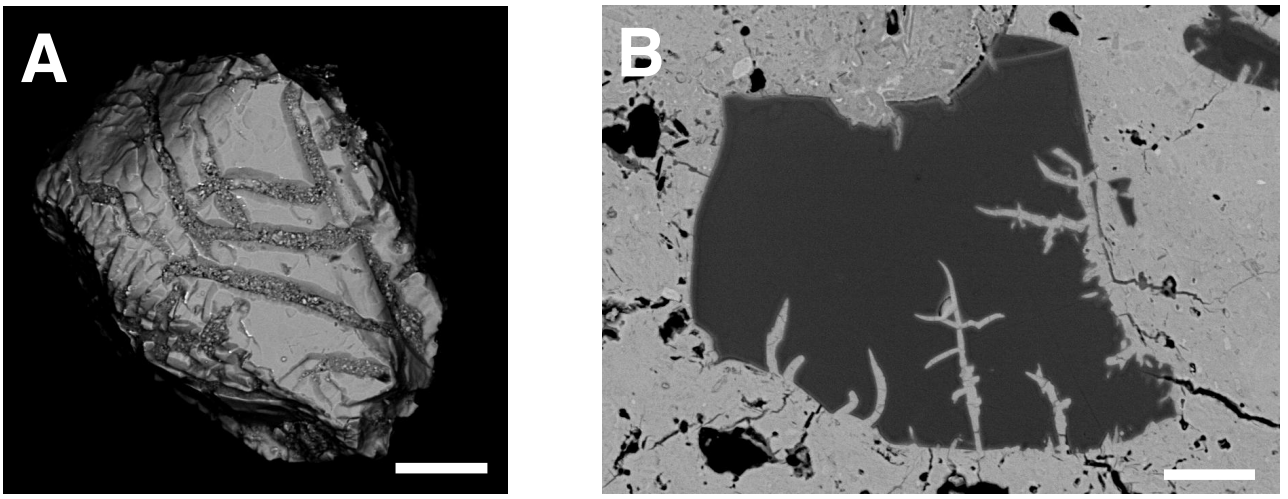

FIGURE 4. SEM images of (**a**) a hand-picked chromite grain from the Oxisol sample at 160 cm and (**b**) a chromite grain embedded in a fine matrix of secondary Fe-oxyhydroxides on a thin section of the Oxisol sample at 80 cm. Both show weathered grains with dissolution features filled with secondary Fe-oxyhydroxides. Scale bar is 30 and 10 µm for **a** and **b**, respectively.

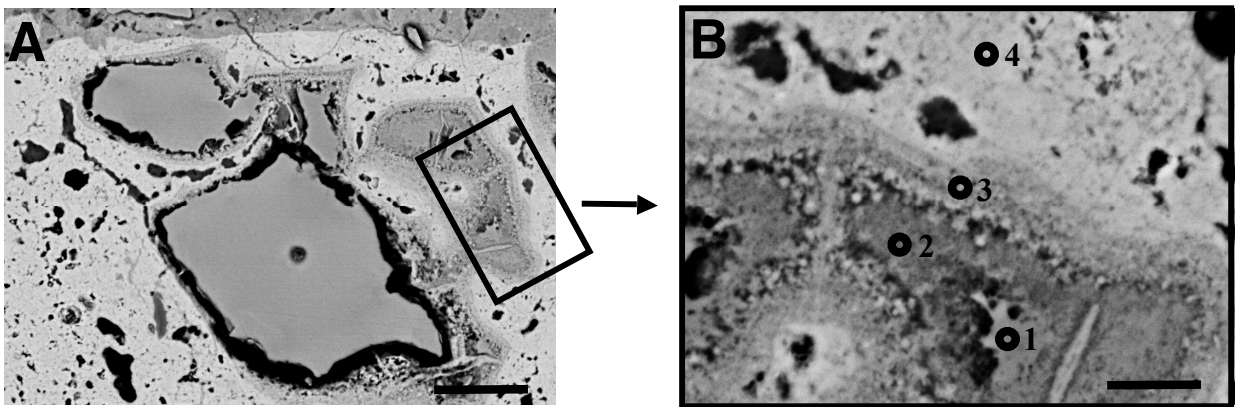

FIGURE 5. SEM images of a deeply weathered chomite grain in the Oxisol sample at 80 cm depth. Circles labeled 1 to 4 in **b** indicate the location of the EPMA analyses reported in Table 2. The two large gray grains in **a** correspond to significantly less weathered chromite. Scale bar is 10 and 2 µm on **a** and **b**, respectively.

TABLE 2. SEM-EDS analyses (wt% oxides) of the different parts identified around the deeply weathered chromite grain depicted in Figure 5

Analysis	SiO_2	MgO	FeO	Cr_2O_3	Al_2O_3	Na_2O	Total
1	0.0	4.3	23.7	65.7	5.3	1.0	100
2	1.1	1.9	38.4	50.5	5.8	0.8	100*
3	1.8	0.0	49.6	43.2	5.4	0.0	100
4	1.9	0.0	91.5	3.0	3.6	0.0	100

Notes: The detection limit on SEM-EDS analyses is estimated at 0.2 wt%.
* This analysis also contains 1.5 wt% SO_2, which makes the sum to 100 wt%.

to the oxidation of Cr^{3+} to the more soluble Cr^{6+}.

All these results suggest that chromite can act as a significant source of Cr through subsequent dissolution upon extensive weathering. Considering the small amounts of secondary Fe-oxyhydroxides and the lack of reactivity of secondary silicates in the case of soils developed upon temperate or Mediterranean weathering of mafic or ultramafic rocks (Oze et al. 2004a; Soubrand-Colin et al. 2007), this dissolution of chromite might represent a risk for the environment. However, in the case of Oxisols, our results indicate that the dispersion of Cr released upon chromite dissolution is likely limited because of subsequent trapping by large amounts of secondary Fe-oxyhydroxides. Considering this latter point, the actual quantification of the partitioning of Cr between chromite and secondary Fe-(hydr) oxides appears an important issue concerning the speciation of Cr in the studied Oxisol samples. Such quantification has been performed by EXAFS spectroscopy, as detailed below.

Quantitative speciation of Cr in the studied samples and crystal-chemical behavior upon tropical weathering of the ultramafic bedrock

In the bedrock sample: Importance of the serpentine component. The EXAFS spectrum at the Cr *K*-edge of the bedrock sample is significantly different from those of the Oxisol samples (Fig. 6), which suggests a different Cr speciation between these two. Comparison with EXAFS spectra of various model compounds shows that the EXAFS spectrum of the bedrock sample is similar to that of the natural Cr-bearing serpentine, despite some

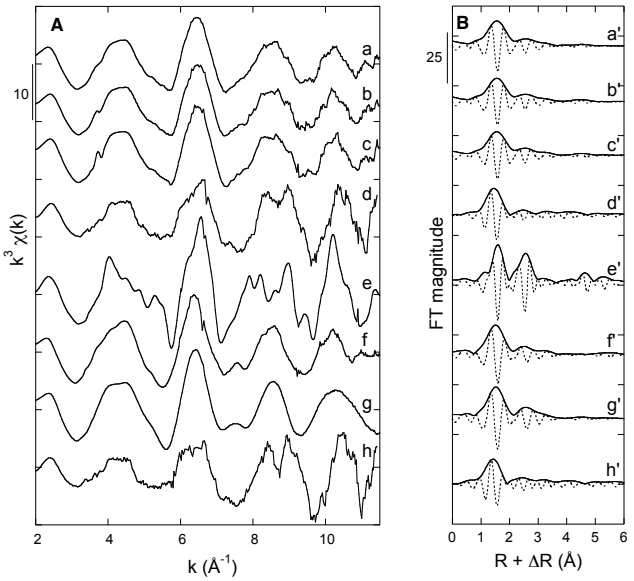

FIGURE 6. (**A**) Cr *K*-edge EXAFS spectra and (**B**) RDF functions of the studied samples [(**a**) Oxisol 10 cm, (**b**) Oxisol 80 cm, (**c**) Oxisol 160 cm, and (**d**) bedrock] and selected model compounds [(**e**) natural chromite, (**f**) synthetic Cr-bearing goethite, (**g**) synthetic Cr-bearing hematite, and (**h**) synthetic Cr-bearing serpentine].

slight differences (Figs. 6d and 6h). This comparison suggests that Cr speciation in the bedrock is dominated by a molecular environment similar to that of Cr in serpentine, although another component cannot be excluded. This hypothesis is in agreement with EPMA data, which indicate the occurrence of significant amounts of Cr in lizardite in this sample [$(Mg_{2.2}Fe_{0.3}Ni_{0.09}Al_{0.07}Cr_{0.02}Ca_{0.02})Si_{2.05}O_5(OH)_4$]. However, SEM observations indicate the occurrence of chromite in this sample, and this component cannot be excluded from the possible Cr speciation because of its high Cr content [$(Fe_{0.39}Mg_{0.60}Mn_{0.01})(Cr_{1.01}Al_{0.98})O_4$]. Finally, EPMA analyses also indicate that enstatite can host significant amounts of Cr, [$(Mg_{0.87}Fe_{0.08}Al_{0.04}Ca_{0.02}Cr_{0.01})SiO_3$], which suggests that this mineral must also be considered as a potential candidate for the additional Cr component. Unfortunately, the quantitative analysis of the EXAFS spectrum of the bedrock sample with the LC-LSF fitting procedure could not be performed because no EXAFS spectrum of synthetic or natural Cr-bearing enstatite was available in our set of model compounds. However, the strong similarities between the EXAFS spectra of the bedrock sample and the natural Cr-bearing serpentine emphasize the importance of the serpentine component on Cr speciation in the bedrock. Considering the higher resistance of this mineral to weathering, compared to olivine and enstatite, such a major contribution of Cr-bearing serpentine on the whole speciation of Cr suggests that the major part of Cr has been released at the latest stage of tropical weathering of the ultramafic bedrock. This late release of Cr might explain the moderate leaching of this element upon tropical weathering of ultramafic rocks because it occurred in a weathering environment where secondary Fe-oxyhydroxides had already abundantly precipitated. This efficiency of secondary Fe-oxyhydroxides to reduce the leaching of Cr released upon weathering of primary Cr-bearing silicate is highlighted in the following section.

In the Oxisol samples: Importance of the secondary Fe-oxyhydroxides. EXAFS spectra at the Cr *K*-edge of the studied Oxisol samples are very similar (Fig. 6), which indicates that Cr speciation is similar in these samples. Comparison with the EXAFS spectra of the model compounds shows a strong similarity with the synthetic Cr-bearing goethite and the Cr-bearing hematite. The EXAFS spectrum of chromite does not fit because it is much more structured than those of the Oxisol samples (Fig. 6). These comparisons indicate that Cr speciation in the Oxisol samples is similar to that of Cr incorporated within the crystal lattices of goethite and/or hematite, which is in agreement with EPMA and SEM-EDS analyses. They also suggest that Cr in chromite does not correspond to the major molecular environment for Cr in the Oxisol samples. Results of the quantitative analysis using the LC-LSF fitting procedure indicate that the best fits are obtained with a mixture of Cr-bearing goethite, chromite, and Cr-bearing hematite (Fig. 7 and Table 3). These quantitative results indicate that the main host for Cr is goethite (from 56 to 63 wt% of total Cr), followed by chromite (from 18 to 22 wt% of total Cr), and then hematite (from 10 to 12 wt% of total Cr) (Table 3). This result is in agreement with the significant concentration of Cr found by EPMA in secondary Fe-oxyhydroxides, which are particularly abundant in the Oxisols samples. Although chromite is much more enriched in Cr, this Cr-rich mineral is not the most abundant species in these samples. The minor change in Cr speciation observed between each Oxisol sample

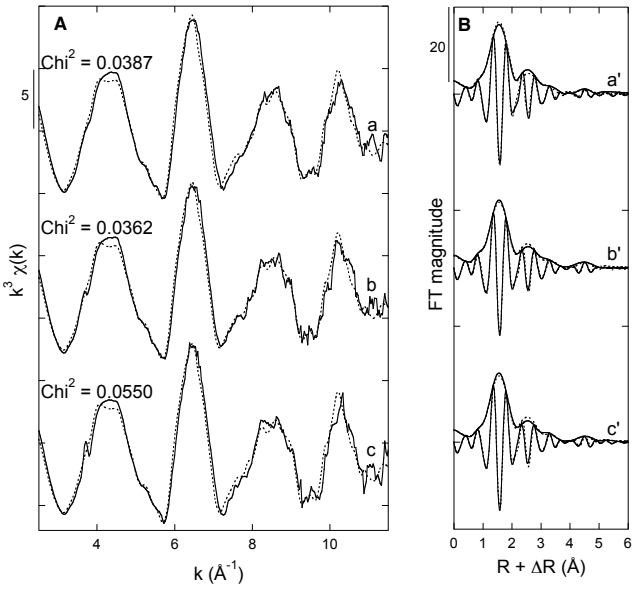

FIGURE 7. (**A**) Experimental (solid lines) Cr *K*-edge EXAFS spectra and (**B**) RDF functions of the studied Oxisol samples [(**a**) 10 cm, (**b**) 80 cm, and (**c**) 160 cm] compared to their LSF fits (dotted lines).

TABLE 3. Percentages of EXAFS spectra of model compounds obtained from the LSF procedure performed on the studied Oxisol samples

	Cr-goethite	Chromite	Cr-hematite	Cr-serpentine
Oxisol-10 cm	45	24	21	–
Oxisol-80 cm	40	26	21	–
Oxisol-160 cm	41	29	17	–

Notes: The sum of all components for each sample was let free.

is in agreement with mineralogical and chemical observations that underline the overall homogeneity of the Oxisol (Fig. 1 and Table 1). These results emphasize the importance of secondary Fe-oxyhydroxides (especially goethite, here) on the trapping of Cr released from primary Cr-bearing silicates upon tropical weathering of the bedrock. These secondary Fe-oxyhydroxides also probably play a significant role in limiting the leaching of Cr due to the later chemical weathering of primary chromite in the bedrock. This importance of secondary Fe-oxyhydroxides on Cr speciation in Oxisols is different from the predominance of Cr-spinels found in soils developed upon temperate or Mediterranean weathering of mafic or ultramafic rocks (Oze et al. 2004a; Soubrand-Colin et al. 2007). It is likely related to the larger relative enrichment of Fe in the Oxisols because of the stronger leaching of soluble elements like Mg and Si upon tropical weathering. The importance of secondary Fe-oxyhydroxides has already been proposed by Becquer et al. (2003, 2006) in Gerric Ferrasols from New Caledonia, but it has never been demonstrated and quantified as reported here.

Redox behavior of Cr upon weathering of the bedrock

Since the geochemical behavior and the toxicity of Cr are strongly dependent on its redox state, this parameter was monitored by XANES spectroscopy in both synthetic and natural samples to emphasize a possible change upon weathering of primary Cr-bearing minerals. The XANES spectrum of the bedrock sample exhibits a main pre-edge peak at 5990 eV and a much smaller one at 5993 eV (Fig. 8). As already explained, the XANES spectrum of Cr^{3+} in a centrosymmetric octahedral environment is characterized by two weak pre-edge peaks at 5990 and 5993 eV (Gaudry et al. 2007; Juhin et al. 2008). The occurrence of these two peaks on the XANES spectrum of the bedrock sample then indicates that Cr is only present as Cr^{3+} in this sample. The XANES spectra of the Oxisol samples also exhibit these two pre-edge peaks at 5990 and 5993 eV, but the one at 5993 eV is significantly more intense than in the bedrock sample (Fig. 8). As already explained, the peak at 5990 eV should be more intense than that at 5993 eV in the case of Cr^{3+} in a regular octahedral environment (Gaudry et al. 2007; Juhin et al. 2008). The larger magnitude of the peak at 5993 eV on the XANES spectra of the Oxisol samples might then be considered as indicative of small amounts of Cr^{6+}, which is characterized by an intense pre-edge peak at 5993 eV (Peterson et al. 1997; Huggins et al. 1998). However, comparison with the synthetic Cr^{3+}-bearing goethite indicates that the pre-edge peak at 5993 eV in this latter model compound is more intense than in the Oxisol samples. This higher intensity of the pre-edge peak at 5993 eV in Cr-bearing goethite is likely related to the distortion of the Cr^{3+} octahedral site, as already explained. Such a distortion of the structural network of goethite when Cr^{3+} is substituted for Fe^{3+} is in agreement with the changes in the lattice parameters reported by Schwertmann and Carlson (1994) and by Schwertmann et al. (2000) for Cr-doped goethite, compared to goethite. Since EXAFS data indicate that the major part of Cr is located in Cr-bearing goethite in the Oxisol samples (Table 3), the intensity of the pre-edge peak at 5993 eV on the XANES spectra of these samples is then more likely related to distortion of the octahedral site of Cr^{3+} within the structural network of Cr^{3+}-bearing goethite, rather than to the occurrence of tetrahedral Cr^{6+}. These observations then suggest that no significant oxidation occurred for Cr released after the dissolution of the Cr^{3+}-bearing primary minerals from the bedrock. This absence of oxidation of Cr

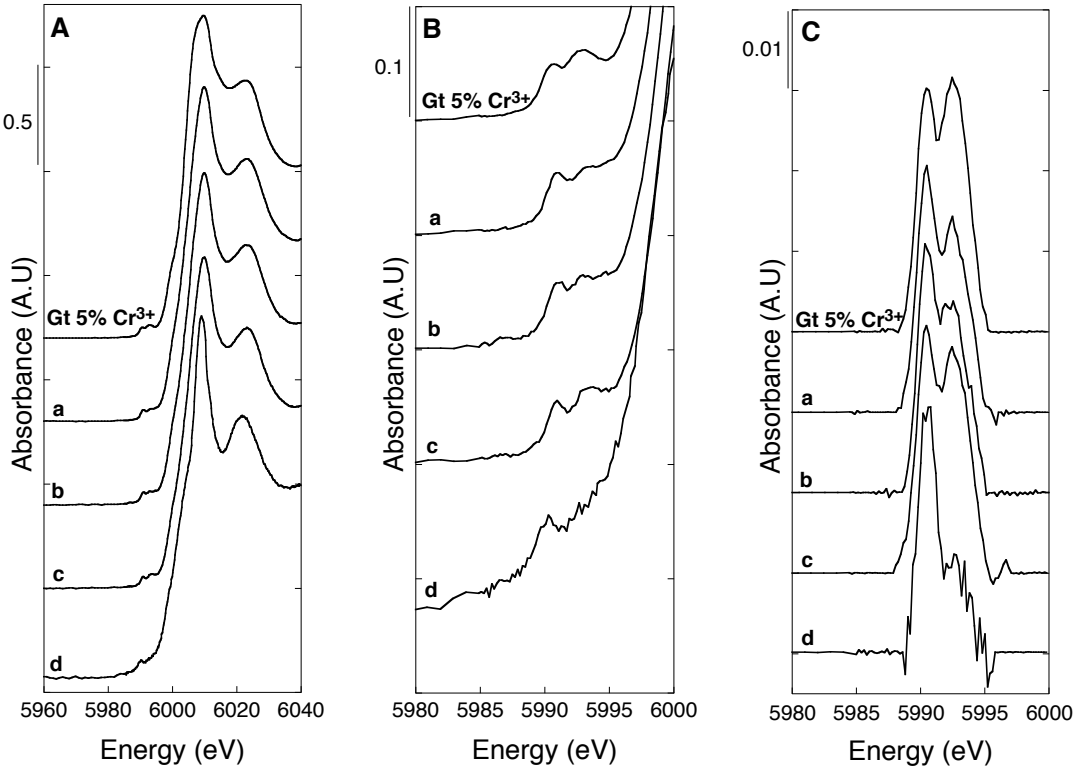

FIGURE 8. (**A**) Normalized bulk, (**B**) pre-edge region zoomed, and (**C**) background substracted pre-edge zoomed region Cr *K*-edge XANES spectra of the studied Oxisol samples [(**a**) 10 cm, (**b**) 80 cm, and (**c**) 160 cm], (**d**) the bedrock sample, and the synthetic Cr^{3+}-bearing goethite model compound.

emphasizes the contrasted redox behavior between this element and Fe, which initially occurred as Fe^{2+} in the primary minerals (forsterite, enstatite, and chromite) of the bedrock and was then subsequently oxidized to Fe^{3+} before precipitating as the identified secondary Fe-oxyhydroxides (goethite and hematite). Such a contrasted redox behavior between both elements is likely due to the higher redox potential of the $HCrO_4^-/CrOH^{2+}$ and $CrO_4^{2-}/Cr(OH)_3$ couples (E_H^0 = +1.1 and +1.34 V, respectively) compared to that of the Fe^{3+}/Fe^{2+} couple (E_H^0 = +0.77 V), which prevents oxidation of Cr^{3+} in solutions in contact with the atmosphere where E^0 is rarely above +0.9 V (Stumm and Morgan 1996). In aerated solutions, Fe^{2+} can then be oxidized to Fe^{3+}, while Cr can remain in its reduced form (Cr^{3+}).

As suggested by the results of previous laboratory (Manceau and Charlet 1992; Fendorf et al. 1993; Weaver and Hochella 2003; Feng et al. 2006; Murray and Tebo 2007) and field studies (Cooper 2002; Becquer et al. 2006), the occurrence of oxidized Cr in soils is likely related to that of Mn oxides. These Mn oxides are also suspected to play a significant role on the chemical weathering of chromite (Oze et al. 2007), as observed in the studied Oxisol. The absence of oxidized Cr in the Oxisol might then be related to the supposed small amounts of Mn oxides, as suggested by the low Mn concentrations (Table 1) and lack of detection by XRD, SEM, and EPMA. However, it might also be due to the enhanced mobility of Cr^{6+}, which is less retained on surfaces of soil components than is Cr^{3+} (Fendorf 1995; Oze et al. 2004b). If some Cr^{3+} has been oxidized to Cr^{6+}, this latter species would then have been leached from the Oxisol and its previoius presence in the studied samples might not be obvious. These considerations indicate that further evaluation of the potential of Mn oxides to generate oxidized Cr in soils developed upon weathering of mafic and ultramafic rocks necessitates more detailed studies focused on both the actual mechanisms involved and the chemistry of soil solutions.

Acknowledgments

This research was funded by the CNRS-INSU "Ecosphère continentale" program through the project "Biogéochimie des éléments métalliques (Fe, Ni, Cr, Mn, and Co) dans le continum sol–eau–microorganismes–plante des écosystèmes latéritiques de Nouvelle-Calédonie: activités anthropiques vs. cycle naturel," which is dedicated to Nicolas Perrier. The authors thank M. Fialin and F. Couffignal from the Centre de Microanalyses CAMPARIS (University Pierre et Marie Curie, Paris, France) for their help during EPMA analyses, S. Borensztajn from the Laboratoire Interfaces et Systèmes Electrochimiques–LISE (University Pierre et Marie Curie, Paris, France) for his assistance during SEM-EDS observation and analyses and the technical staff of ELETTRA (Italy) for their support during XANES analyses. This is IPGP contribution no. 2448.

References cited

Becquer, T., Petard, J., Duwig, C., Bourdon, E., Moreau, R., and Herbillon, A.J. (2001) Mineralogical, chemical and charge properties of Geric Ferralsols from New Caledonia. Geoderma, 103, 291–306.

Becquer, T., Quantin, C., Sicot, M., and Boudot, J.P. (2003) Chromium availability in ultramafic soils from New Caledonia. Science of the Total Environment, 301, 251–261.

Becquer, T., Quantin, C., Rotte-Capet, S., Ghanbaja, J., Mustin, C., and Herbillon, A.J. (2006) Sources of trace metals in Ferralsols in New Caledonia. European Journal of Soil Science, 57, 200–213.

Bish, D.L. and Reynolds, J. (1989) Sample preparation for X-ray diffraction. In D.L. Bish and J.E. Post, Eds., Modern Powder Diffraction, 20, p. 73–99. Reviews in Mineralogy, Mineralogical Society of America, Chantilly, Virginia.

Coleman, P.J. (1980) Plate tectonics background to biogeographic development in the southwest Pacific over the last 100 million years. Palaeogeography, Palaeoclimatology, Palaeoecology, 31, 105–121.

Cooper, G.R.C. (2002) Oxidation and toxicity of chromium in ultramafic soils in Zimbabwe. Applied Geochemistry, 17, 981–986.

Cornell, R.M. and Schwertmann, U. (2003) The iron oxides: Structure, reactions, occurrences and uses, 2nd edition. Wiley-VCH Verlag, Weinheim.

Doelsch, E., Basile-Doelsch, I., Rose, J., Masion, A., Borschneck, D., Hazemann, J.L., Saint Macary, H., and Bottero, J.Y. (2006) New combination of EXAFS spectroscopy and density fractionation for the speciation of chromium within an Andosol. Environmental Science and Technology, 40, 7602–7608.

Fendorf, S.E. (1995) Surface reactions of chromium in soils and waters. Geoderma, 67, 55–71.

Fendorf, S.E. and Li, G. (1996) Kinetics of chromate reduction by ferrous iron. Environmental Science and Technology, 30, 1614–1617.

Fendorf, S.E., Sasoski, R.J. and Burau, R.G. (1993) Competing metal-ion influences on chromium(III) oxidation by birnessite. Soil Science Society of America Journal, 57, 1508–1515.

Feng, X.H., Zhai, L.M., Tan, W.F., Zhao, W., Liu, F., and He, J.Z. (2006) The controlling effect of pH on oxidation of Cr(III) by manganese oxide minerals. Journal of Colloid and Interface Science, 298, 258–266.

Garnier, J., Quantin, C., Martins, E.S., and Becquer, T. (2006) Solid speciation and availability of chromium in ultramafic soils from Niquelândia, Brazil. Journal of Geochemical Exploration, 88, 206–209.

Garrels, R.M. and Christ, C.L. (1965) Solutions, Minerals and Equilibria. Harper and Row, New York.

Gaudry, E., Cabaret, D., Brouder, C., Letard, I., Rogalev, A., Wilhlem, F., Jaouen, N., and Sainctavit, P. (2007) Relaxations around the substitutional chromium site in emerald: X-ray absorption experiments and density functional calculations. Physical Review B, 76, 094110.

He, Y.T., Bigham, J.M., and Traina, S.J. (2005) Biotite dissolution and Cr(VI) reduction at elevated pH and ionic strength. Geochimica et Cosmochimica Acta, 69, 3791–3800.

Huggins, R.J., Craig, J.R., and Gibbs, G.V. (1979) Systematics of the spinel structure type. Physics and Chemistry of Minerals, 4, 317–339.

Isaure, M.-P., Laboudigue, A., Manceau, A., Sarret, G., Tiffreau, C., Trocellier, P., Lamble, G., Hazemann, J.-L., and Chateigner, D. (2002) Quantitative Zn speciation in a contaminated dredged sediment by μ-PIXE, μ-SXRF, EXAFS spectroscopy and principal component analysis. Geochimica et Cosmochimica Acta, 66, 1549-1567.

Juhin, A., Calas, G., Cabaret, D., Galoisy, L., and Hazemann, J.L. (2008) Structural relaxation around substitutional Cr^{3+} in pyrope garnet. American Mineralogist, 93, 800–805.

Kendelewicz, T., Liu, P., Doyle, C.S., and Brown Jr., G.E. (2000) Spectroscopic study of the reaction of aqueous Cr(VI) with Fe_3O_4 (111) surfaces. Surface Science, 469, 144–163.

Loyaux-Lawniczak, S., Refait, P., Ehrhardt, J.J., Lecomte, P., and Genin, J.M. (2000) Trapping of Cr by formation of ferrihydite during the reduction of chromate ions by Fe(II)-Fe(III) hydroxysalt green rusts. Environmental Science and Technology, 34, 438–443.

Manceau, A. and Charlet, L. (1992) X-ray absorption spectroscopic study of the sorption of Cr(III) at the oxide-water interface: I. Molecular mechanism of Cr(III) oxidation on Mn oxides. Journal of Colloid and Interface Science, 148, 425–442.

Manceau, A., Lanson, B., Schlegel, M.L., Harge, J.C., Musso, M., Eybert-Berard, L., Hazemann, J.L., Chataignier, D., and Lamble, G.M. (2000) Quantitative Zn speciation in smelter-contaminated soils by EXAFS spectroscopy. American Journal of Science, 300, 289–343.

Merkle, R.K.W., Loubser, M., and Graser, P.P.H. (2004) Incongruent dissolution of chromite in lithium tetraborate flux. X-Ray Spectrometry, 33, 222–224.

Murray, K.J. and Tebo, B.M. (2007) Cr(III) is indirectly oxidized by the Mn(II)-oxidizing bacterium *Bacillus* sp. Strain SG-1. Environmental, Science and Technology, 41, 528–533.

Myers, N., Mittermeier, R.A., Mittermeier, C.G., da Fonseca, G.A.B., and Kent, J. (2000) Biodiversity hotspots for conservation priorities. Nature, 403, 853–858.

Nriagu, J.O. (1988) Production and uses of chromium. In J.O. Nriagu and E. Nieboer, Eds., Natural and Human Environments, 359 p. Wiley Interscience, New York.

Ostergren, J.D., Brown Jr., G.E., Parks, G.A., and Tingle, T.N. (1999) Quantitative speciation of lead in selected mine tailings from Leadville, CO. Environmental Science and Technology, 33, 1627–1636.

Oze, C., Fendorf, S., Dennis, K.B., and Coleman, R.G. (2004a) Chromium geochemistry in serpentinized ultramafic rocks and serpentine soils from the franciscan complex of California. American Journal of Science, 304, 67–101.

Oze, C., Fendorf, S., Bird, D., and Coleman, R.G. (2004b) Chromium geochemistry of serpentine soils. International Geology Review, 46, 97–126.

Oze, C., Bird, D., and Fendorf, S. (2007) Genesis of hexavalent chromium from natural sources in soil and groundwater. Proceedings of the National Academy of Science, 104, 6544–6549.

Perrier, N., Ambrosi, J.P., Colin, F., and Gilkes, R.J. (2006) Biogeochemistry of a regolith: The New Caledonian Koniambo ultramafic massif. Journal of Geochemical Exploration, 88, 54–58.

Peterson, M.L., Brown Jr., G.E., Parks, G.A., and Stein, C.L. (1997) Differential redox and sorption of Cr(III/VI) on natural silicate and oxide minerals: EXAFS and XANES results. Geochimica et Cosmochimica Acta, 61, 3399–3412.

Proctor, J. (2003) Vegetation and soil and plant chemistry on ultramafic rocks in the tropical Far East. Perspectives in Plant Ecology, Evolution and Systematics, 6, 105–124.

Quantin, C., Becquer, T., Rouiller, J.H., and Berthelin, J. (2002) Redistribution of metals in a New Caledonia ferralsol after microbial weathering. Soil Science Society of America Journal, 66, 1797–1804.

Ravel, B. and Newville, M. (2005) Athena, artemis, hephaestus: Data analysis for X-ray absorption spectroscopy using IFEFFIT. Journal of Synchrotron Radiation, 12, 537–541.

Rooney, P.C., Zhao, F.J., and McGrath, S.P. (2006) Phytotoxicity of nickel in a range of European soils: Influence of soil properties, Ni solubility, and speciation. Environmental Pollution, 145, 596–605.

Sarret G.; Balesdent J.; Bouziri L.; Garnier J-M.; Marcus M.A.; Geoffroy N.; Panfili F.; Manceau A. (2004) Zn speciation in the organic horizon of a contaminated soil by micro-X-ray fluorescence, micro- and powder-EXAFS spectroscopy, and isotopic dilution. Environmental Science and Technology, 38, 2792–2801.

Scheinost, A.C., Kretzschmar, R., Pfister, S., and Roberts, D.R. (2002) Combining selective sequential extractions, X-ray absorption spectroscopy, and principal component analysis for quantitative zinc speciation in soil. Environmental Science and Technology, 36, 5021–5028.

Schwertmann, U. and Carlson, L. (1994) Aluminum influence on iron oxides: XVII. Unit-cell parameters and aluminum substitution of natural goethites. Soil Science Society of America Journal, 58, 256–261.

Schwertmann, U. and Latham, M. (1986) Properties of iron oxides in some New Caledonian oxisols. Geoderma, 39, 105–123.

Schwertmann, U., Friedl, J., Stanjek, H., and Schulze, D.G. (2000) The effect of Al on Fe oxides: XIX. Formation of Al-substituted hematite and ferrihydrite at 25 °C and pH 4 to 7. Clays and Clay Minerals, 48, 159–172.

Soubrand-Colin, M., Néel, C., Bril, H., Grosbois, C., and Caner, L. (2007) Geochemical behaviour of Ni, Cr, Cu, Zn, and Pb in an Andosol-Cambisol clomosequence on basaltic rocks in the French Massif Central. Geoderma, 137, 340–351.

Stumm, W. and Morgan, J.J. (1996) Aquatic Chemistry, 3rd edition. Wiley Interscience, New York.

Szulczewski, M.D., Helmke, P.A., and Bleam, W.F. (2001) XANES spectroscopy studies of Cr(VI) reduction by thiols in organosulfur compounds and humic substances. Environmental Science and Technology, 35, 1134–1141.

Traoré, D., Beauvais, A., Chabaux, F., Pfeiffert, C., Parisot, J.C., Ambrosi, J.P., and Colin, F. (2008) Chemical and physical transfers in an ultramafic rock weathering profile: Part 1. Supergene dissolution of Pt-bearing chromite. American Mineralogist, 93, 22–30.

Voegelin, A., Pfister, S., Scheinost, A.C., Marcus, M.A., and Kretzschmar, R. (2005) Changes in zinc speciation in field soil after contamination with zinc oxide. Environmental Science and Technology, 39, 6616–6623.

Weaver, R.M. and Hochella Jr., M.F. (2003) The reactivity of seven Mn-oxides with Cr^{3+}_{aq}: A comparative analysis of a complex, environmentally important redox reaction. American Mineralogist, 88, 2016–2027.

Webb, S. (2004) Sixpack: A graphical user interface for XAS analysis using IFEFFIT. Physica Scripta, T115, 1011–1014.

Weng, L.P., Wolthoorn, A., Lexmond, T.M., Temminghoff, E.J.M., and Van Riemsdijk, W.H. (2004) Understanding the effects of soil characteristics on phytotoxicity and bioavailability of nickel using speciation models. Environmental Science and Technology, 38, 156–162.

Williams, A.G. and Scherrer, M.M. (2001) Kinetics of Cr(VI) reduction by carbonate green rust. Environmental Science and Technology, 35, 3488–3494.

Winterer, M. (1997) XAFS: A data analysis program for materials science. Journal de Physique IV, 7, C2.243–C2.244.

Manuscript received August 11, 2008
Manuscript accepted January 8, 2009
Manuscript handled by Barry Bickmore